https://doi.org/10.1364/BOE.8.005594

Research Article | Vol. 8, No. 12 | 1 Dec 2017 | BIOMEDICAL OPTICS EXPRESS 5594

Biomedical Optics EXPRESS

# Detection of optical activity with diode-integrated hyperbolic metasurfaces

**JOSEPH S. T. SMALLEY,[1,2,*] FELIPE VALLINI,[1] AND YESHAIAHU FAINMAN[1]**

[1]*Department of Electrical & Computer Engineering, University of California San Diego, La Jolla, CA, 92037, USA*

[2]*Department of Mechanical Engineering, University of California Berkeley, Berkeley, CA 94720, USA*

[*]*jstsmalley@berkeley.edu*

**Abstract:** We present an analytical technique for designing integrated polarized light-emitting diodes (LEDs) and polarization-sensitive photodiodes (PD) based on hyperbolic metasurfaces (HMS) for the detection of optical activity. Leveraging effective medium theory and the scattering matrix method, we first derive the conditions for optimizing the transmission efficiency of an LED-integrated HMS and the absorption efficiency of a PD-integrated HMS. We then propose using a differential detection technique with orthogonally oriented PD-integrated HMS to measure optical activity in an extremely compact volume. Finally, we perform an estimation of system performance and find that, relative to state-of-the-art polarimeters, a reduction of complexity can be achieved without sacrificing resolution. The results hold merit for reducing the size and cost of polarimeters and associated polarimetric sensing systems, which play vital roles in the pharmaceutical and biomedical sciences.



**OCIS codes:** (130.5440) Polarization-selective devices; (280.1415) Biological sensing and sensors; (260.2065) Effective medium theory; (160.1585) Chiral media; (160.3918) Metamaterials; (130.3120) Integrated optics devices.

## References and links

1. L. D. Barron, *Molecular Light Scattering and Optical Activity* (Cambridge University Press, 1982).
2. P. Salvadori and F. Ciardelli, "An Introduction to Chiroptical Techniques: Basic Principles, Definitions, and Applications," in *Fundamental Aspects and Recent Developments in Optical Rotatory Dispersion and Circular Dichroism*, F. Ciardelli and P. Salvadori, eds. (Heyden & Son Ltd, 1973), pp. 3–26.
3. K. Vollhardt and N. Schore, "Stereoisomers," in *Organic Chemistry: Structure and Function* (W. H. Freeman and Company, 2007), pp. 168–214.
4. A. Rodger and B. Norden, *Circular Dichroism and Linear Dichroism* (Oxford University, 1997).
5. E. E. Narimanov and A. V. Kildishev, "Metamaterials: Naturally hyperbolic," Nat. Photonics **9**, 214–216 (2015).
6. L. Ferrari, C. Wu, D. Lepage, X. Zhang, and Z. Liu, "Hyperbolic metamaterials and their applications," Prog. Quantum Electron. **40**, 1–40 (2015).
7. A. A. High, R. C. Devlin, A. Dibos, M. Polking, D. S. Wild, J. Perczel, N. P. de Leon, M. D. Lukin, and H. Park, "Visible-frequency hyperbolic metasurface," Nature **522**(7555), 192–196 (2015).
8. J. S. T. Smalley, F. Vallini, S. A. Montoya, L. Ferrari, S. Shahin, C. T. Riley, B. Kanté, E. E. Fullerton, Z. Liu, and Y. Fainman, "Luminescent hyperbolic metasurfaces," Nat. Commun. **8**, 13793 (2017).
9. H. Yuan, X. Liu, F. Afshinmanesh, W. Li, G. Xu, J. Sun, B. Lian, A. G. Curto, G. Ye, Y. Hikita, Z. Shen, S. C. Zhang, X. Chen, M. Brongersma, H. Y. Hwang, and Y. Cui, "Polarization-sensitive broadband photodetector using a black phosphorus vertical p-n junction," Nat. Nanotechnol. **10**(8), 707–713 (2015).
10. J. S. Smalley, F. Vallini, and Y. Fainman, "Nanoscale Polarimeter Enabled by Luminescent Hyperbolic Metasurfaces," in *Optics in the Life Sciences Congress* (OSA, 2017), p. BoS2A.5.
11. W. Li, Z. J. Coppens, L. V. Besteiro, W. Wang, A. O. Govorov, and J. Valentine, "Circularly polarized light detection with hot electrons in chiral plasmonic metamaterials," Nat. Commun. **6**, 8379 (2015).
12. Y. Zhao, A. N. Askarpour, L. Sun, J. Shi, X. Li, and A. Alù, "Chirality detection of enantiomers using twisted optical metamaterials," Nat. Commun. **8**, 14180 (2017).
13. G. M. Whitesides, "The origins and the future of microfluidics," Nature **442**(7101), 368–373 (2006).
14. S. M. Rytov, "Electromagnetic properties of a finely stratified medium," J. Exp. Theor. Phys. **2**, 466 (1956).
15. Y.-L. Liao and Y. Zhao, "Design of wire-grid polarizer with effective medium theory," Opt. Quantum Electron. **46**, 641–647 (2014).
16. "n k database: Aluminum Compounds," http://www.ioffe.ru/SVA/NSM/nk/index.html#AlComp.
17. K. M. McPeak, S. V. Jayanti, S. J. P. Kress, S. Meyer, S. Iotti, A. Rossinelli, and D. J. Norris, "Plasmonic films can easily be better: Rules and recipes," ACS Photonics **2**(3), 326–333 (2015).
18. G. M. Hale and M. R. Querry, "Optical constants of water in the 200 nm to 200 um wavelength region," Appl.

#301433 https://doi.org/10.1364/BOE.8.005594
Journal © 2017 Received 5 Jul 2017; revised 27 Oct 2017; accepted 8 Nov 2017; published 14 Nov 2017

Biomedical Optics EXPRESS

Opt. **12**(3), 555–563 (1973).
19. M. A. Green, "Self-consistent optical parameters of intrinsic silicon at 300 K including temperature coefficients," Sol. Energy Mater. Sol. Cells **92**, 1305–1310 (2008).
20. F. Krayzel, R. Polles, A. Moreau, M. Mihailovic, and G. Granet, "Simulation and analysis of exotic non-specular phenomena," J. Eur. Opt. Soc. **5**, 10025 (2010).
21. J. Sun, M. I. Shalaev, and N. M. Litchinitser, "Experimental demonstration of a non-resonant hyperlens in the visible spectral range," Nat. Commun. **6**, 7201 (2015).
22. J. Graeme, *Photodiode Amplifiers: Op Amp Solutions* (McGraw-Hill, 1996).
23. R. C. Weast, *Handbook of Chemistry and Physics*, 55th ed. (CRC Press, 1974).

## 1. Introduction

Optical activity arises due to the interaction between the electric and magnetic dipoles of chiral molecules [1,2]. When a preponderance of right- or left-handed chiral molecules is present in a solution, linearly polarized light passing through the solution rotates, providing a fingerprint from which information about the solution can be inferred. Polarimetry is the fundamental technique used to characterize chiral solutions, enabling knowledge of the concentration of enantiomer-pure solutions, the enantiomer purity of a solution of known concentration, and the specific rotation of new substances [1–3]. Its importance is widespread, finding application in toxicology and drug discovery, for example.

Typical polarimeters consist of a white light source, linear polarizer, sample cell, and polarization analyzer, along with control electronics. State-of-the-art polarimeters directly measure circular dichroism of substances by alternately measuring the absorption of left- and right-handed circular polarization [4]. While a direct measurement provides accurate results, it requires numerous bulky and expensive optical components, leading to systems that occupy benchtops and cost thousands of dollars. A natural question is therefore whether recent innovations in nanophotonics can be leveraged to reduce the size and cost of state-of-the-art polarimeters, without diminishing their performance.

Hyperbolic metamaterials (HMM) are a class of naturally existing [5] and artificially engineered [6] material that simultaneously exhibit hyperbolic and elliptical dispersion for waves of different polarization. Experimentally, the dispersion discrepancy leads to extreme polarization anisotropy. Because most HMM consist of vertically alternating metallic and dielectric layers, observation of polarization anisotropy tends to depend strongly on the incident angle of an interacting wave and require oblique incidence. However, lateral multilayer HMM of nanoscale thickness, also known as hyperbolic metasurfaces (HMS) [7], exhibit extreme anisotropy at normal incidence. For example, extreme linear dichroism (LD) at near-infrared frequencies was demonstrated in a luminescent HMS (LuHMS) based on indium gallium arsenide phosphide (InGaAsP) multiple quantum wells nanostructured with silver (Ag) [8].

While naturally existing 2D materials also exhibit LD [9], the magnitude and bandwidth of LD is generally fixed in 2D materials, whereas it can be tailored in engineered HMS. Furthermore, HMS based on III-V compounds tend to be more environmentally stable and may be integrated with control electronics to serve as compact, robust sources and detectors of polarized light. In this letter we present an architecture for detecting optical activity based on engineering the LD in diode-integrated HMS [10]. We apply our method to the case of a yellow light-emitting diode (LED) and silicon photodiode (PD) at the vacuum wavelength of $\lambda_0 = 589$ nm, and show how differential detection of linearly polarized light passing through a chiral solution can lead to a measure of optical activity.

While utilization of metamaterials for detection of optical activity has previously been reported [11,12], to the best of our knowledge, our work constitutes the first proposal of a fully integrated source, sample, and detector for an ultra-compact optical activity detection system [10]. By fully integrating the individual components necessary for detecting optical activity, the design enables sensing systems without bulky optical elements, reducing size and cost. This work therefore represents an important application of HMS and LuHMS of potential value to the pharmaceutical and biomedical communities.

Biomedical Optics EXPRESS

## 2. Design overview

Experimentally, optical activity may be observed as the rotation of the plane of polarization of polarized light passing through chiral molecules dissolved in solution [1]. The specific rotation of molecules in solution is given by

$$\left[\alpha_T^{\lambda_0}\right] = \frac{\theta_{\text{rot}}}{cd} \tag{1}$$

where $\lambda_0$ is the probe wavelength and $T$ is the temperature. Commonly used reference values for the wavelength and temperature are 589 nm and 20°C, respectively. The concentration, $c$, and light-matter interaction length, $d$, are expressed in units of g $mL^{-1}$ and dm, respectively, such that the specific rotation has units of ° $dm^{-1}$ mL $g^{-1}$. For substances with known concentration, Eq. (1) can be used to determine the optical activity. Conversely, for enantiomer-pure solutions of known optical activity, Eq. (1) can be used to determine their concentration.

Use of Eq. (1) in the determination of optical activity necessarily requires a source of linearly polarized light. Conventional polarimeters typically rely upon filtering a broadband white light source to pass 589 nm light, followed by a polarizer to obtain linearly polarized light. For maximum polarization purity, the ratio between transmissions for orthogonally polarized waves should be as high as possible. Use of an integrated LED-HMS and HMS-PD simplifies the design of a polarimetric system.

A schematic of the envisioned polarized LED and polarization-sensitive PD integrated with a microfluidic channel is shown in Fig. 1. The upper HMS polarizes otherwise randomly polarized emission from the LED. Light exiting the upper HMS becomes polarized along the direction of the optical axis of the HMS, which is the x direction in Fig. 1. The wave then interacts with molecules dissolved in the microfluidic channel. If a preponderance of right- or left-handed chiral molecules exists, the plane of polarization will be rotated. After traversing the solution, light interacts with the lower HMS, which consists of two HMS with orthogonally oriented optical axes, each at a ± 45° angle with respect to the optical axis of the upper HMS. Rotation of the originally x-polarized light leads to a preferential absorption in one of the photodiodes adjacent to the lower HMS. For example, In Fig. 1, a + 45° rotation leads to a significantly larger transmission through the left lower HMS relative to the right lower HMS. Note that the boundary of the microfluidic channel, usually made of polydimethylsiloxane (PDMS) [13], physically separates the solution from both the upper and lower HMS, which is indicated by the black region in the cross-section of Fig. 1. Additionally, in Fig. 1 the surfaces of the metallic elements, rather than their edges, are in contact with the microfluidic channel and diode layers.

Biomedical Optics EXPRESS

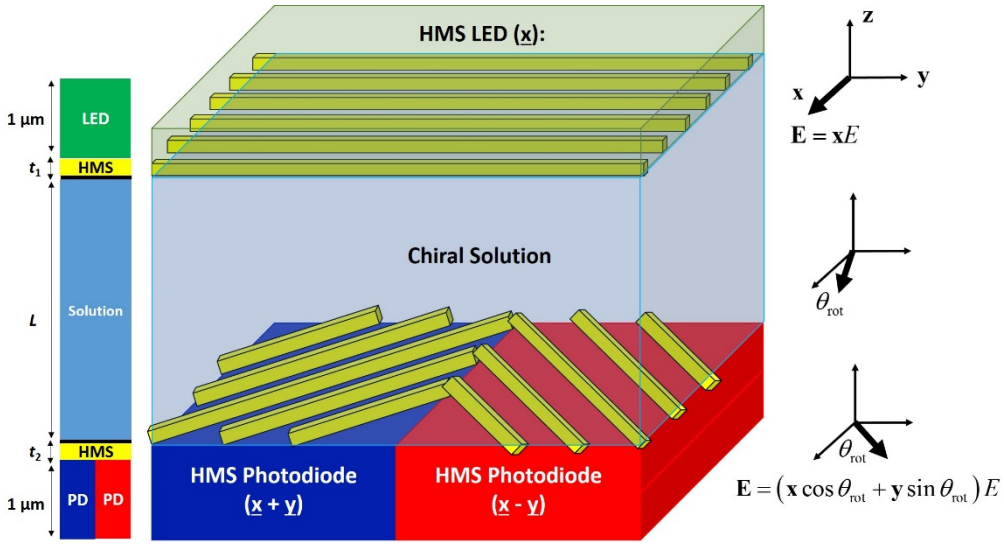


Fig. 1. Schematic of integrated polarized LED, microfluidic channel and orthogonally-oriented polarization-sensitive photodiodes for detection of optical activity. The optical axis of the upper HMS corresponds to the **x** unit vector. For the lower HMS, the optical axes are (left lower) $\mathbf{x}2^{-1/2} + \mathbf{y}2^{-1/2}$ and (right lower) $\mathbf{x}2^{-1/2} - \mathbf{y}2^{-1/2}$. The thickness of the upper and lower HMS, $t_1$ and $t_2$, respectively, are design parameters, along with the metal-to-air ratio in the HMS. The black regions between the HMS and solution in the cross-section indicate physical separation between the HMS and solution. Dimensions not to scale.

The electromagnetic response of the HMS is usually described in terms of the effective permittivity tensor,

$$\boldsymbol{\varepsilon} = \left[\varepsilon_{\parallel}, 0; 0, \varepsilon_{\perp}\right] \tag{2}$$

where the elements parallel and normal to the optical axis depend on the permittivity of the metal, $\varepsilon_M$, and dielectric, $\varepsilon_D$, and the metal fill fraction, $\rho$, through [14]

$$\varepsilon_{\parallel} = \varepsilon_{\parallel}' + i\varepsilon_{\parallel}'' = \varepsilon_M \varepsilon_D / \left[\rho\varepsilon_D + (1-\rho)\varepsilon_M\right] \tag{3}$$

$$\varepsilon_{\perp} = \varepsilon_{\perp}' + i\varepsilon_{\perp}'' = \rho\varepsilon_M + (1-\rho)\varepsilon_D \tag{4}$$

Because of losses, and possibly gain [8], in the constituent materials, the effective permittivity elements are generally complex, with the single and double primes denoting real and imaginary parts, respectively. Given the dispersion of the constituent metallic and dielectric materials, maximizing the LD of the HMS therefore consists of identifying the optimal values of the HMS parameters, $\rho$ and the thickness, $t$.

For a Type II HMS [8], in which $\varepsilon'_{\parallel}>0$ and $\varepsilon'_{\perp}<0$, as occurs for a Ag/air system in the visible and near-infrared, the effective refractive indices are given by

$$n_{\parallel}' = \sqrt{|\varepsilon_{\parallel}|}\cos\left[\tan^{-1}\left(\frac{\varepsilon_{\parallel}''}{\varepsilon_{\parallel}'}\right)\frac{1}{2}\right] \tag{5}$$

$$n_{\parallel}'' = \sqrt{|\varepsilon_{\parallel}|}\sin\left[\tan^{-1}\left(\frac{\varepsilon_{\parallel}''}{\varepsilon_{\parallel}'}\right)\frac{1}{2}\right] \tag{6}$$

Biomedical Optics EXPRESS

$$n'_{\perp} = -\sqrt{|\varepsilon_{\perp}|}\sin\left[\tan^{-1}\left(\frac{\varepsilon''_{\perp}}{\varepsilon'_{\perp}}\right)\frac{1}{2}\right] \tag{7}$$

$$n''_{\perp} = \sqrt{|\varepsilon_{\perp}|}\cos\left[\tan^{-1}\left(\frac{\varepsilon''_{\perp}}{\varepsilon'_{\perp}}\right)\frac{1}{2}\right] \tag{8}$$

Minimal reflection and maximal transmission for waves polarized parallel to the HMS optical axis occurs under the quarter wave condition when the thickness of the HMS, $t$, is

$$t = m\frac{\lambda_0}{4n'_{\|}}, \quad m = 1,3,5,... \tag{9}$$

and

$$n'_{\|} = \sqrt{n_1 n_2} \tag{10}$$

where $n_1$ and $n_2$ are the real refractive indices of the top and bottom layers adjacent to the HMS [15]. For waves polarized perpendicular to the HMS optical axis, the reflection increases and transmission decreases monotonically with HMS thickness.

## 3. Design implementation

Because the optical activity of compounds is commonly measured using the sodium D line, we illustrate our method by maximizing the LD of HMS at $\lambda_0$ = 589 nm. In principle, however, the method can be applied for an arbitrary wavelength, so long as the effective medium approximation remains valid. Intuitively, the constituent metal should be a good reflector at the wavelength of interest. Therefore, we consider the lowest loss plasmonic metal, Ag, in combination with air. Note that results for an HMS with Au or Al as the constituent metal would be similar. This configuration enables fabrication with a single lithographic step and avoids etching, which degrades the quality of the light-emitting material. The source of light is an LED whose active region is the compound semiconductor aluminum gallium indium phosphide ($Al_{0.15}Ga_{0.35}In_{0.5}P$), the alloy content of which can be tuned for emission at 589 nm. Silicon is used for the detection of light after passing through the chiral substance.

The permittivites used in the following calculations are 11.52 for AlGaInP [16], –15.59 + 0.37i for Ag [17], 1.77 for the solution [18], and 15.72 + 0.17i for Si [19]. The bounding diode layers above and below the HMS are 1 μm thick and a normally incident wave is launched from the top of the upper layer (see Fig. 1). The use of a purely real permittivity for AlGaInP is justified because the population inversion necessary for electroluminescence leads to a transparent medium. Losses associated with highly doped regions for the carrier injection uniformly reduce the transmission for all polarizations. The thin PDMS layer separating the HMS and solution (black regions in cross-section of Fig. 1) is ignored because it is optically transparent and affects TM and TE polarization identically at normal incidence.

### *3.1 Optimization of degree-of-linear-polarization and efficiency*

Figure 2(a)-2(b) shows the analytical design of the Ag/air HMS. The Ag fraction is first varied to identify when Eq. (10) is satisfied. As shown in Fig. 2(a), this occurs at $\rho$ = 0.73 and $\rho$ = 0.76 for the upper HMS (between AlGaInP and solution) and lower HMS (between solution and Si), respectively. Next, we use Eq. (9) to predict the HMS thickness at which the transmission is maximal for the parallel polarization. Figure 2(b) shows that this occurs at approximately $t$ = 70 nm and $t$ = 210 nm for both the upper and lower HMS. We then employ the scattering matrix method (SMM) [20] to calculate transmission (T), reflection (R), and

Biomedical Optics EXPRESS

absorption (A) of the TM (parallel) and TE (perpendicular) waves as a function of HMS thickness. The results, shown in Fig. 2(c) for the upper HMS, verify maximal transmission of the TM wave for thickness of 70 nm and 210 nm, and the monotonic decrease of TE transmission. By comparing the TM transmission peaks near 70 nm and 210 nm, a small amount of absorption due to the HMS is observed. Figure 2(d) shows that the degree of linear transmission (DOLT), a measure of LD defined as

$$\mathrm{DOLT} \equiv \left| \frac{\mathrm{T(TM)} - \mathrm{T(TE)}}{\mathrm{T(TM)} + \mathrm{T(TE)}} \right|, \tag{11}$$

increases exponentially with the HMS thickness. The primary reason for this is the exponentially increasing reflection of the TE wave with thickness.

To meet the additional requirements of efficient operation and manufacturability, the HMS thickness should correspond to a quarter wave condition, and be as thin as possible to avoid absorption of the TM wave and fabrication challenges associated with forming high aspect ratio structures. For $t$ = 70 nm, DOLT = 0.993 and T(TM) = 0.991, while for $t$ = 210 nm, DOLT>0.999999 and T(TM) = 0.973 If the metal is deposited via sputtering, then selecting a thickness of 70 nm ensures a practically realizable aspect ratio of less than 3:1, assuming a 100 nm period with a ~75 nm Ag block and a ~25 nm air trench [8]. However, as shown in Section 3.3, a thicker HMS is desirable to mitigate errors in detection. In this case, electroplating can be used to form the metal blocks. For example, in [21], 300 nm thick gold blocks were formed by electroplating, with block thickness and block-to-block spacing sufficiently small to warrant use of effective medium theory.

Results from similar calculations for the lower HMS are shown in Fig. 2(e)-2(f). Here it is desired to maximize and minimize absorption of the TM and TE waves, respectively. As seen in Fig. 2(e) absorption of the TM waves peaks near $t$ = 60 nm and $t$ = 190 nm. We define the degree of linear absorption (DOLA) as

$$\mathrm{DOLA} \equiv \left| \frac{\mathrm{A(TM)} - \mathrm{A(TE)}}{\mathrm{A(TM)} + \mathrm{A(TE)}} \right|, \tag{12}$$

which is shown in Fig. 2(f) as a function of HMS thickness. Initially the DOLA rises exponentially with HMS thickness due to the reflection of the TE wave, followed by an oscillatory behavior due to the reflection of the TM wave. For $t$ = 60 nm, DOLA = 0.949 and A(TM) = 0.914, while for $t$ = 190 nm, DOLA = 0.965 and A(TM) = 0.917. Selecting a thickness of 190 nm therefore maximizes both the DOLA and absorption of TM waves.

Biomedical Optics EXPRESS

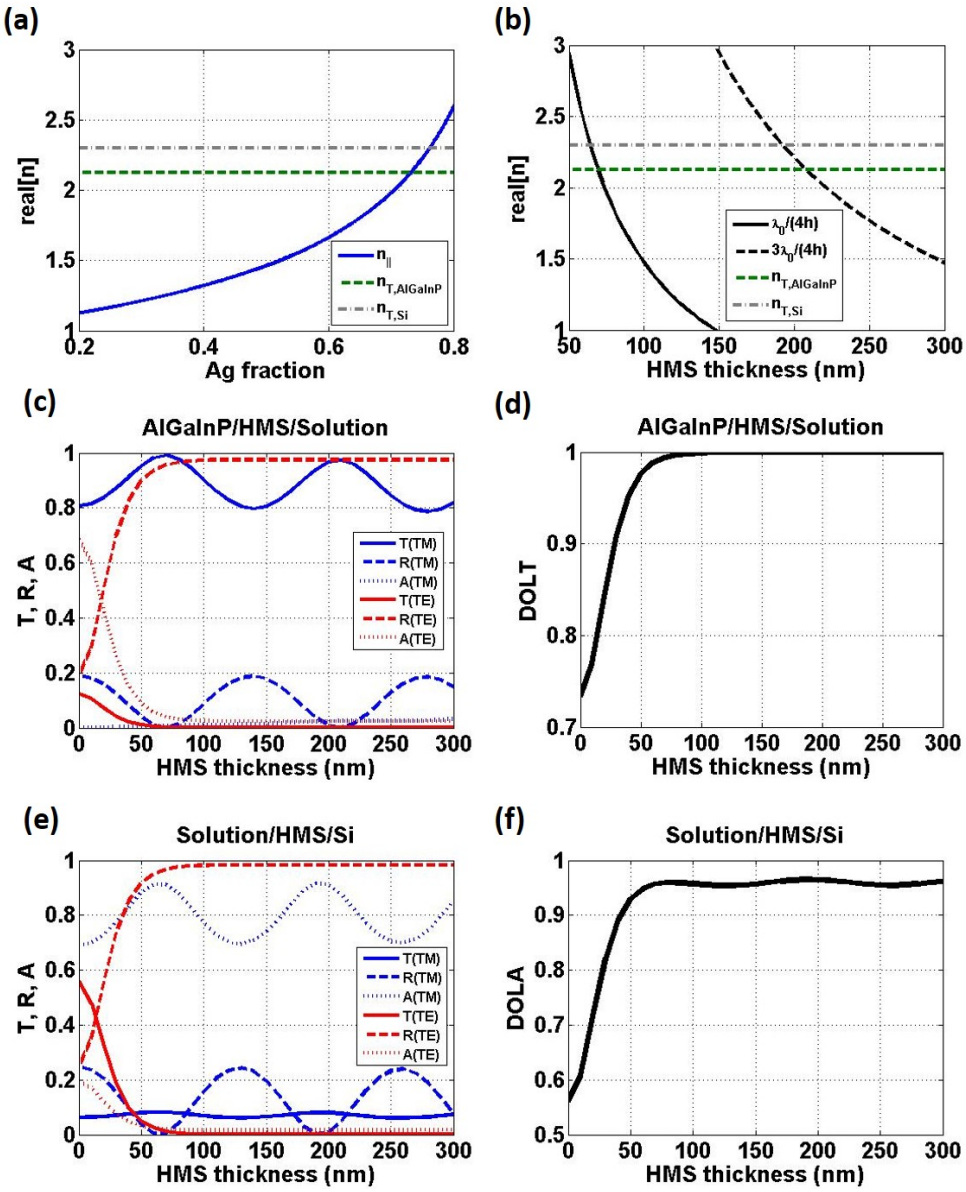


Fig. 2. (a) Parallel (TM) effective index as a function of Ag fraction in HMS and values of the optimal index calculated from Eq. (10) for reference. (b) Quarter wave index as a function of thickness. (c) Transmission, reflection, and absorption of TM and TE waves and (d) degree of linear transmission as functions of the HMS thickness for the AlGaInP/HMS/solution system. (e) Transmission, reflection, and absorption of TM and TE waves and (f) degree of linear transmission as functions of the HMS thickness for the solution/HMS/Si system.

### *3.2 Differential detection*

As indicated by Fig. 1, detection of optical activity relies upon measuring the difference in photocurrent, $I_p$, generated in segmented diodes underneath orthogonally oriented HMS. Figure 3 presents a basic circuit diagram for a differential measurement of these photocurrents [22]. The cathode (n-contact) is shared between both HMS-photodiodes and corresponds to the ground of the circuit. A split-anode (p-contact) configuration, which is commonly found in light-based position sensors, is used to connect each HMS-photodiode to

Biomedical Optics EXPRESS

a different operation amplifier (op-amp), wherein each photocurrent is converted into a voltage. A third op-amp then receives the two voltages as inputs and, in conjunction with a resistance, $R_f$, delivers an output voltage proportional to the difference in photocurrents, $V_O = (Ip_1\text{-}Ip_2)R_f$ [22]. The polarity of $V_O$ indicates whether the rotation is left-hand or right-hand and the magnitude is proportional to the degree of rotation.

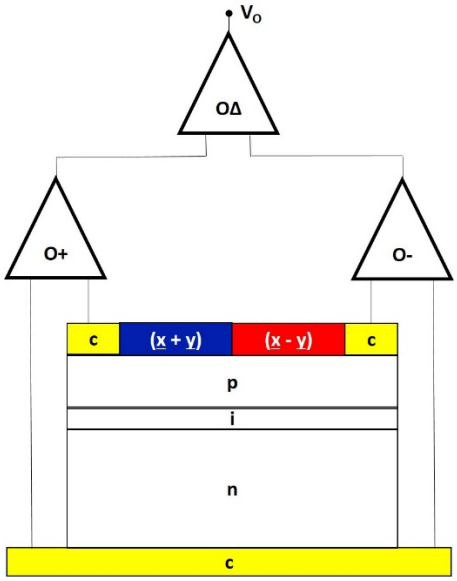


Fig. 3. Split-anode photodiode with orthogonally oriented HMS and op-amp circuit for differential detection. The output voltage, $V_O$, of OΔ is proportional to the difference in photocurrents generated underneath the orthogonal HMS (c = contact, p = p-doped region, n = n-doped region, i = intrinsic region, O = op amp).

### 3.3 Estimation of system performance

To assess the potential utility of the proposed system for detection of optical activity, we estimate the performance in terms of the achievable resolution.

Consider the upper HMS specified in Fig. 2, with $\rho = 0.73$ and $t = 70$ nm. Assume 20 mW optical power output from the AlGaInP active region, 10 mW each of which may be considered TM and TE polarization. Additionally, assume 90% transmission, the balance of which accounts for free-carrier losses associated with highly doped regions in the AlGaInP. Using the results of Fig. 2(c), we obtain the optical power entering the solution from the upper HMS of $P_0 = 8.92$mW and $P_0 = 0.025$ mW for the TM and TE polarization, respectively. Because the TE power is non-negligible, we immediately conclude that use of $t = 210$ nm were preferable, which leads to initial TM and TE power of 8.78 mW and $1.2\text{x}10^{-6}$ mW, respectively.

In the absence of any chiral or absorbing substance, light experiences no rotation, and the generated photocurrents reaching the O + and O- op-amps will be identical. The photocurrents entering the op amps, O + (O-), are given by $I_{p\,+\,(-)} = RP_{+(-)}$, where $R$ is the responsivity and $P_+$ ($P_-$) is the power absorbed in the Si after traversing the $\underline{x} + \underline{y}$ ($\underline{x}\text{-}\underline{y}$) segment of the lower HMS. That is, $P_{+(-)} = A_{+(-)}P_0/2$, where $A_{+(-)}$ is the absorption in the Si layer. We take $R = 0.4$ A $W^{-1}$, representative of a conventional silicon photodiode and for simplicity assume that $R$ is identical for each diode segment. Under the ideal case that DOLA = 1, $A_+$ and $A_-$ are proportional to $\cos^2(45°\text{-}\theta_{rot})$ and $\sin^2(45°\text{-}\theta_{rot})$, respectively, where $-45° < \theta_{rot} < 45°$ is defined in Fig. 4(a)-4(b), as the angle of rotation with respect to the x-axis after traversal of the chiral solution length, $L$. Figure 4(c)-4(d) presents the differential

Biomedical Optics EXPRESS

photocurrent, $\Delta I_P = I_{P,+} - I_{P,-} = (A_+ - A_-)RP_0/2$, as a function of $\theta_{rot}$ for this ideal case. The scale of $|\max(\theta_{rot})|$ decreases from 45° in Fig. 4(c) to 0.001° in Fig. 4(d) for visual clarity. From Fig. 4(c)-4(d) we see that the resolution in detection of $\theta_{rot}$ scales linearly with $\Delta I_p$. Hence, 1.0° resolution requires ability to detect $\Delta I_p = 0.4$ mA, while 0.001° resolution requires ability to detect $\Delta I_p = 0.4$ μA. For this latter case, use of a high-impedance resistor with $R_f = 1.0$ MΩ in conjunction with the op-amp circuit of Fig. 3 would lead to an output voltage of $V_O = R_f \Delta I_p = 0.4$ V, which is an easily measurable quantity.

Because the DOLA is less than unity practically, $I_{p+}$ and $I_{p-}$ become modified. Namely in the extreme case of a 45° rotation, assuming use of a 60 nm lower HMS, the TM and TE waves experience 91.3% and 2.4% total absorption, respectively, rather than 100% and 0%. To assess the effect of non-ideal DOLA on the resolution, we calculate the unwanted photocurrent generated by non-zero TE absorption. Accounting for absorption in the HMS, the unwanted current for $t = 60$ nm is 25 μA, which, assuming a minimum desired signal-to-noise ratio of 10, jeopardizes measuring better than 1.0° resolution. On the other hand for $t = 190$ nm, the unwanted photocurrent becomes 1.9 nA, which is more than two orders of magnitude less than the 400 nA required for a 0.001° resolution in the ideal case. Therefore, a thickness on the order of 200 nm for both the upper and lower HMS is a requirement to achieve a resolution competitive with the state-of-the-art.

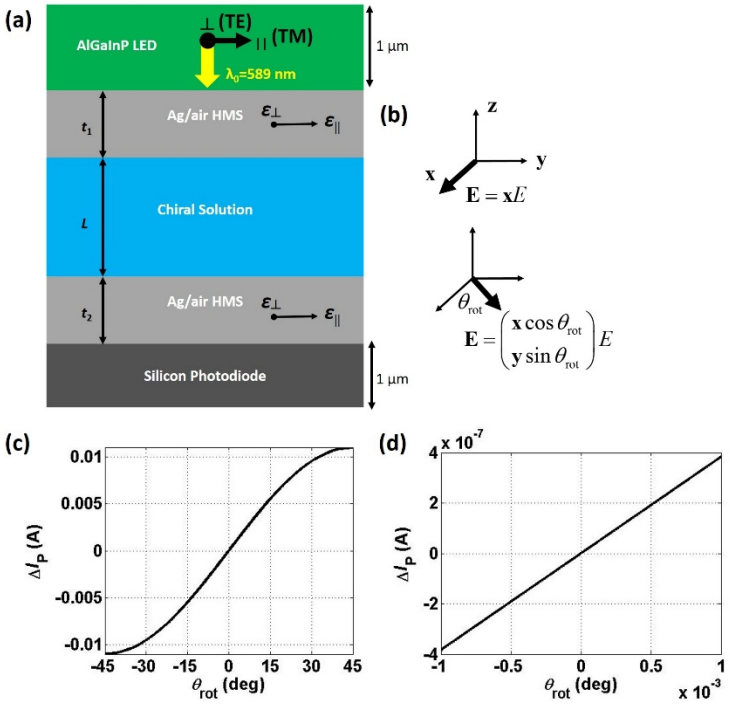


Fig. 4. (a) Cross-sectional schematic of polarimeter. (b) Definition of $\theta_{rot}$ and electric field vector after passing upper HMS and chiral solution. (c-d) Differential current, $\Delta I_P = I_{P,1} - I_{P,2}$ as a function of $\theta_{rot}$ with $|\max(\theta_{rot})|$ = (b) 45° and (c) 0.001°.

As a practical example of the utility of the proposed ultra-compact polarimeter we analyze the performance in measuring the optical activity of D-glucose [23]. D-glucose is known to exhibit a specific rotation of + 52.7° $dm^{-1}$ $cm^3$ $g^{-1}$. Assuming a solution of D-Glucose in water with 0.9 g $mL^{-1}$ solubility, linearly polarized light will rotate + 4.79° after traversing an interaction length of 0.1 dm. From Fig. 4(c), we can deduce that the differential photocurrent will be ≈215 μA. If L-glucose, the synthetic enantiomer of g-Glucose, were present in the

Biomedical Optics EXPRESS

solution, a smaller differential photocurrent would be expected and the relative concentrations of both molecules could be back-calculated.

## 4. Discussion

Thus far we have assumed monochromatic and normally incident plane wave operation of the diode-integrated HMS. Obviously this is a limitation of the proposed design.

If broadband operation is essential, then emerging 2D materials that exhibit natural anisotropy could be employed [9]. However, use of black phosphorus, for example, in place of an Ag/air HMS, suffers from the tradeoff of a significantly lower polarization extinction ratio, which would lead to a much smaller DOLP. Therefore the choice of bandwidth versus DOLP must be made with the ultimate sensing goal in mind.

Additionally, design of the HMS based on a normally incident plane wave from the AlGaInP active layer is a first order approximation. While some of the emitted power from the LED inevitably approaches the upper HMS at an oblique angle, the normally incident component has the highest transmission and has thus been used in this analysis.

We also assumed use of a PIN photodiode underneath the receiver HMS. This choice is somewhat arbitrary in the sense that other photodetection architectures could be employed. For example, if an increased responsivity were desired at the expense of a longer response time, a phototransistor architecture could be employed. Nonetheless, the general principle of differential detection between orthogonally oriented HMS atop the detection plane remains a compelling design goal.

## 5. Conclusion

We have proposed a new architecture to detect optical activity in an extremely compact and robust footprint. The architecture consists of a polarized LED and polarization-sensitive photodiode, both of which are enabled by HMS designed by effective medium theory. Optical rotation is determined by measuring the differential photocurrents in photodiodes integrated with orthogonally-oriented HMS. We assessed the performance of the proposed system and showed that measurements of 0.001° resolution appear feasible with the use of sufficiently thick HMS. The proposed sensing system thus has the advantage of a smaller footprint and potential cost while maintaining state-of-the-art performance.

## Funding

The authors acknowledge funding from the National Science Foundation (NSF), Award No. 1507146, “Exploring the Frontiers of Photonic Device Size, Speed, and Efficiency using Gain-Enhanced Multifunctional Metamaterials (GEMMs),” the Office of Naval Research Multidisciplinary Research Initiative, Award No. N00014-13-1-0678, “Near-field energy efficient communications and computing,” and the NSF Center for Integrated Access Networks, Award No. EEC-0812072.

## Disclosures

The authors declare that there are no conflicts of interest related to this article.